JᴍM RAPIDS

Bifurcation analysis of bubble-induced convection in a horizontal liquid layer: role of forces on bubbles

Kotaro Nakamura[1],[†], Harunori N. Yoshikawa[2], Yuji Tasaka[1] and Yuichi Murai[1]

[1]Laboratory for Flow Control, Hokkaido University, Sapporo 060-8628, Japan

[2]Université Côte d'Azur, CNRS, Institut de Physique de Nice, 06100 Nice, France

We investigate with a two-fluid model the convections developing in a gas–liquid two-phase flow, which consists of a horizontal liquid layer subject to the injection of monodisperse gas bubbles at the bottom. The convections develop in either whole- or multi-layered modes, once the gas injection flux exceeds a critical value (Nakamura *et al.*, *Phys. Rev.* E, vol. 102, 2020, 053102). We determine the nonlinear evolution of these modes of flows with varying injection flux and find that the whole- and multi-layered modes develop through subcritical and supercritical bifurcations, respectively. The formation of gas plumes is observed in both cases when the nonlinearity is significant. Examining energy transfer from base to perturbation flows, we show that the lift forces on bubbles play a key role in the bifurcations. While they impede the convections in both subcritical and supercritical bifurcations at weak nonlinearity, the lift forces turn to driving the convections in the subcritical bifurcation as nonlinearity increases.

Key words: buoyancy-driven instability, gas/liquid flow, bifurcation

1. Introduction

Liquid flows with dispersed gas phases have been investigated in various fields of scientific research to understand their complex multi-scale flow structures and to develop novel applications of energy and environmental systems (Lohse 2018). Presence of dispersed bubbles alters turbulent flow structures and induces large-scale liquid circulations (Risso 2018). This pertains to industrial applications of, for example, bubble column reactors (Sommerfeld 2004) used as efficient gas–liquid contactors for enhancement of mass and heat transfer, in which bubbles are injected into a liquid layer from the bottom. The injected

† Present address: Department of Mechanical Engineering, National Institute of Technology, Ube College, Ube 755-8555, Japan. Email address for correspondence: kotaro@ube-k.ac.jp

bubbles rise in liquid due to Archimedean buoyancy forces, exchanging mass and heat at gas–liquid interfaces (Mudde 2005). The two-phase flows in reactors show a variety of flow patterns depending on the bubble size, the gas volume fraction, and the geometric shapes of reactors (Mudde 2005; Risso 2018). When the gas injection flux is small, bubbles ascend with a uniform distribution (Mudde 2005; Ruzicka 2013). At large gas fluxes, the bubble distribution becomes heterogeneous and convective motions occur (Mudde 2005).

The generation of convection in two-phase flow systems with a bubble-rich bottom layer has been modelled as a gravitational instability provoked in an inverse density stratification (Iga & Kimura 2007). Ruzicka & Thomas (2003) elucidated the analogy to the Rayleigh–Bénard (RB) convection. The bubble-induced convection is thus often characterised in the literature by the Rayleigh and Prandtl numbers, Ra and Pr. They are identical to those used for thermal convections but with the bubble residence time $T_R = d/V_\infty$ replacing the thermal diffusion time: $Ra = T_\nu T_R/T_B^2$, $Pr = T_R/T_\nu$, where d is the height of a system, V_∞ is the terminal velocity of a rising bubble, $T_\nu = d^2/\nu$ is the momentum diffusion time with the kinematic viscosity ν of the liquid, and $T_B = \sqrt{d/\varepsilon g}$ is the buoyancy time (ε, the gas volume fraction; g, gravitational acceleration). Iga & Kimura (2007) showed the formation of steady convection rolls at $Ra = 2.5 \times 10^5$ in an experiment with bubbles of approximately 10 µm in diameter. A direct numerical simulation (DNS) based on a point bubble model by Climent & Magnaudet (1999) showed that steady convection rolls developed for $Ra \sim 2.0 \times 10^5$ from an initial two-layer state where a bubble-rich fluid layer underlies a pure liquid layer. These works both mentioned that the selection of the horizontal size of convection rolls is not unique and the size changes depending on randomly determined initial conditions.

Recently, we performed a linear stability analysis of bubble-induced convection (Nakamura *et al.* 2020), assuming an inverse density profile formed spontaneously from the accelerated ascending motion of bubbles (figure 1*a*). The analysis is based on a two-fluid model, in which the added-mass, drag, shear-induced lift and buoyancy forces on bubbles are considered in the momentum exchanges between liquid and gas phases. In contrast to the RB convection, the predicted marginal stability curves $Ra = Ra_m(k)$, where k is the wavenumber of perturbation flows, have two local minima and their relationship varies as function of Pr. Convection rolls of the height of the fluid layer (whole-layered mode, see figure 1*c*-i) are critical for Pr smaller than a threshold Pr^*, while superposed convection rolls (multi-layered mode, see figure 1*c*-ii) are critical otherwise (Nakamura *et al.* 2020). Although the values of Pr^* and Ra_m depend on the radius and the injection velocity of bubbles and on the model of drag coefficient, the qualitative behaviour of the marginal curves and the resulting mode selection remain the same.

The present work aims to reveal the nonlinear development of the whole- and multi-layered modes with a particular focus on their bifurcation behaviour. For this aim, nonlinear flows close to the critical states are computed to draw bifurcation diagrams. In thermal convection of non-Newtonian fluids, the bifurcations depend on the fluid rheology: it can be supercritical as in the RB convection of Newtonian fluids but also subcritical, when shear-thinning effects are significant (Bouteraa *et al.* 2015). The presence of a dispersed solid phase can also alter the type of bifurcation in the RB convection through the variation of the effective viscosity of suspension resulting from the shear-diffusion of suspended particles (Kang, Yoshikawa & Mirbod 2021). By the present investigation, we show that even in the absence of rheological effects the presence of dispersed phase can affect the bifurcation in two-phase flow systems. The considered flow system is isothermal and convection develops from an intrinsic gravitational instability of bubbly flows. Dilute bubbly flows are assumed so that the constitutive law of the continuous
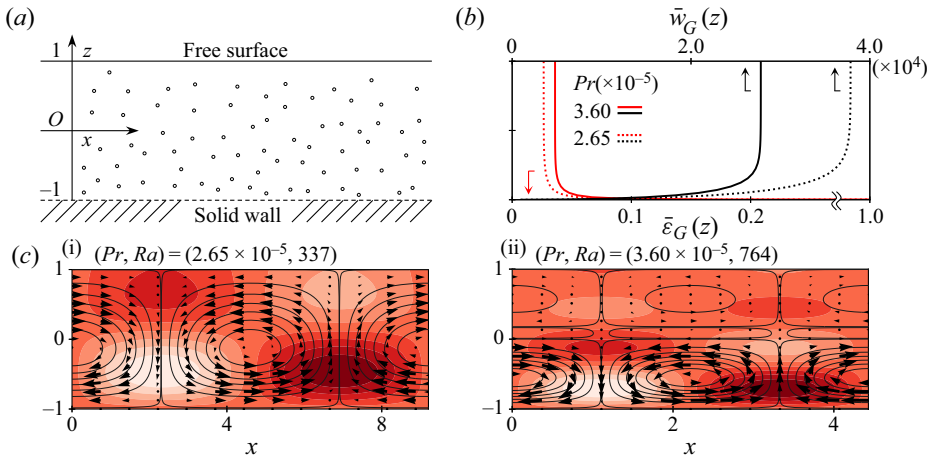
Figure 1. (*a*) Geometric configuration of the problem, (*b*) profiles of bubble rising velocity $\bar{w}_G(z)$ and gas volume fraction $\bar{\varepsilon}_G(z)$ in the base state for different values of Pr, and (*c*) eigenvectors at critical conditions for (i) a whole-layered mode and (ii) a multi-layered mode. The dimensionless bubble injection velocity and bubble radius are set as $w_{G,0} = 1000$ and $r_b = 0.01$, respectively. The perturbation fields of liquid velocity $\boldsymbol{u}'$ are shown by vectors and streamlines. The perturbation fields of gas volume fraction ε'_G are shown by colours. Bubble-rich and bubble-poor cells correspond to red and white zones.

phase remains Newtonian. Following the introduction, we present a brief summary of a mathematical model used in our previous report (Nakamura *et al.* 2020) and describe a numerical method for nonlinear flow determination. The properties of the solution are then explained using bifurcation diagrams showing flow patterns. Finally, we discuss the roles of different forces on bubbles in the nonlinear development of convection.

2. Formulation of the problem

2.1. *Governing equations*

We consider two-dimensional (2-D) bubbly flows in a horizontal fluid layer. Small spherical bubbles are injected into the liquid layer from the bottom wall (figure 1*a*). The injection is assumed uniform in space and constant in time. Injected bubbles rise in the layer due to buoyancy forces and are ejected from the top free surface. We model the dynamics of this immiscible two-phase flow system using the Euler–Euler approach, in which the liquid and gas phases are regarded as two dynamical continua exchanging momentum and energy with each other. Mass and momentum conservations for the two phases are modelled as

$$\frac{\partial \varepsilon_G}{\partial t} + \boldsymbol{\nabla} \cdot (\varepsilon_G \boldsymbol{u}_G) = 0, \tag{2.1a}$$

$$\frac{\mathrm{D}\boldsymbol{u}_G}{\mathrm{D}t} = 3\frac{\mathrm{D}\boldsymbol{u}}{\mathrm{D}t} - \frac{18}{r_b^2}(\boldsymbol{u}_G - \boldsymbol{u}) - (\boldsymbol{u}_G - \boldsymbol{u}) \times (\boldsymbol{\nabla} \times \boldsymbol{u}) + \frac{18}{Pr r_b^2}\boldsymbol{e}_z, \tag{2.1b}$$

$$\boldsymbol{\nabla} \cdot \boldsymbol{u} = 0, \tag{2.1c}$$

$$\frac{\mathrm{D}\boldsymbol{u}}{\mathrm{D}t} = -\boldsymbol{\nabla}p + \Delta\boldsymbol{u} - \frac{9}{Pr r_b^2}\boldsymbol{e}_z + \varepsilon_G \frac{Ra r_b^2}{9Pr}\left(\frac{\mathrm{D}\boldsymbol{u}}{\mathrm{D}t} + \frac{9}{Pr r_b^2}\boldsymbol{e}_z\right), \tag{2.1d}$$

923 R4-3

where ε_G is gas volume fraction, $\boldsymbol{u}_G = u_G \boldsymbol{e}_x + w_G \boldsymbol{e}_z$ and $\boldsymbol{u} = u \boldsymbol{e}_x + w \boldsymbol{e}_z$ are the velocity fields of gas and liquid, and p is the pressure field (see Nakamura *et al.* 2020, and references therein for details). The unit vectors in the x and z directions are denoted by $\boldsymbol{e}_x$ and $\boldsymbol{e}_z$. The differential operator $\mathrm{D}/\mathrm{D}t$ represents $\mathrm{D}\boldsymbol{u}_G/\mathrm{D}t = \partial_t \boldsymbol{u}_G + \boldsymbol{u}_G \cdot \nabla \boldsymbol{u}_G$ and $\mathrm{D}\boldsymbol{u}/\mathrm{D}t = \partial_t \boldsymbol{u} + \boldsymbol{u} \cdot \nabla \boldsymbol{u}$. These equations have been non-dimensionalised with scales d of length, ν/d of velocity and d^2/ν of time. The gas volume fraction has been normalised with a scale $J_{G,0} d/\nu$, where $J_{G,0}$ is the gas injection flux. We have introduced the following four dimensionless parameters:

$$ Pr = \frac{\nu}{V_\infty d} = \frac{9\nu^2}{gR_b^2 d}, \quad Ra = \frac{gd^2 J_{G,0}}{V_\infty^2 \nu} = \frac{81\nu d^2 J_{G,0}}{gR_b^4}, \quad w_{G,0} = \frac{W_{G,0}\, d}{\nu}, \quad r_b = \frac{R_b}{d}, $$

$$ (2.2a\text{--}d) $$

where R_b and $W_{G,0}$ are the radius and the injection velocity of bubbles, respectively. For bubbles of radius 0.5 mm injected into a water layer of thickness 100 mm at room temperature with $W_{G,0} = 20$ mm s^{-1} and $J_{G,0} = 1$ mm s^{-1}, these parameters take values of $Pr = 7.34 \times 10^{-5}$, $Ra = 330$, $w_{G,0} = 1000$, $r_b = 0.01$. Throughout the present work, the dimensionless bubble injection velocity $w_{G,0}$ and bubble radius r_b are fixed at these values. In the gas momentum equation (2.1b), the hydrodynamic diffusion has been omitted, assuming dilute bubbly flows. We have also assumed spherical and non-deformable bubbles in a pure liquid without contamination by surfactants to model drag and shear-induced lift forces and adopt the drag, added-mass and lift coefficients $C_D = 48/Re_b$ (Levich 1962), where $Re_b = 2R_b \|\boldsymbol{u}_G - \boldsymbol{u}\|/\nu$ is the bubble Reynolds number, and $C_A = C_L = 1/2$ (Magnaudet & Eames 2000). This model of C_D describes well bubble motions for $Re_b \sim 30\text{--}400$ (Clift, Grace & Weber 2005), e.g. bubbles of $R_b = 0.5$ mm in a steady ascending motion in water at room temperature. In the liquid mass conservation equation (2.1c) and the liquid momentum equation (2.1d), liquid flows are considered effectively incompressible, as we have assumed dilute bubbly flows. We have also restricted our attention to flows at scales larger than the mean distance between bubbles. The dynamics of the liquid phase is thus affected by bubbles only through the mesoscale reaction force, $\varepsilon_G(\mathrm{D}\boldsymbol{u}/\mathrm{D}t - \boldsymbol{g})$ (Druzhinin & Elghobashi 1998).

The upper surface of the liquid layer is assumed as flat and shear-free for simplicity. At the bottom wall, no-slip conditions on the liquid velocity, constant gas velocity and constant gas flux are imposed:

$$ \frac{\partial u}{\partial z} + \frac{\partial w}{\partial x} = 0, \quad w = 0, \quad \text{at } z = 1, \tag{2.3a} $$

$$ \boldsymbol{u} = \boldsymbol{0}, \quad w_G = w_{G,0}, \quad \varepsilon_G = 1, \quad \text{at } z = -1. \tag{2.3b} $$

2.2. *Base state*

Two-dimensional flows would respect the translational symmetry of the system along the x direction when the gas flux $J_{G,0}$, or the Rayleigh number Ra in the dimensionless description, is small. We thus assume a steady bubbly flow in the homogeneous regime, where the flow fields are laterally uniform:

$$ \boldsymbol{u} = \boldsymbol{0}, \quad \boldsymbol{u}_G = \bar{w}_G(z)\, \boldsymbol{e}_z, \quad \varepsilon_G = \bar{\varepsilon}_G(z). \tag{2.4a\text{--}c} $$

For these fields, (2.1a) and (2.1b) read

$$ \frac{\mathrm{d}}{\mathrm{d}z}(\bar{\varepsilon}_G \bar{w}_G) = 0, \quad \bar{w}_G \frac{\mathrm{d}\bar{w}_G}{\mathrm{d}z} = -\frac{18\bar{w}_G}{r_b^2} + \frac{18}{Pr\, r_b^2}, \tag{2.5a,b} $$

and the boundary conditions (2.3) are reduced to

$$\bar{w}_G = w_{G,0}, \quad \bar{\varepsilon}_G = 1, \quad \text{at } z = -1. \tag{2.6a,b}$$

Some profiles of velocity $\bar{w}_G$ and gas fraction $\bar{\varepsilon}_G$ calculated from (2.5a,b) and (2.6a,b) are shown in figure 1(b). The gas velocity increases toward the terminal velocity V_∞ in a fluid sublayer attached to the wall. Inside the sublayer, the fraction $\bar{\varepsilon}_G$ decreases sharply so that the stratification in the mean density of the liquid–gas mixture is potentially unstable to the gravity.

The profiles of $\bar{w}_G$ and $\bar{\varepsilon}_G$ depend on Pr. At small Pr, the density gradient is small and the unstable sublayer extends over a thick zone of the fluid layer. Our linear stability analysis (Nakamura *et al.* 2020) showed that the whole-layered convection rolls develop when Ra exceeds a critical value (figure 1c-i) for Pr smaller than a threshold Pr^*. For Pr larger than Pr^*, the unstable sublayer is thin, and the multi-layered mode (figure 1c-ii) is selected as a critical state. The value of Pr^* is 3.25×10^{-5} for $(r_b, w_{G,0}) = (0.01, 1000)$. At this Prandtl number, both whole- and multi-layered modes are critical at $Ra = 645$. Similar formation of whole- and multi-layered convection rolls sensitive to density profiles is reported for thermal convections (Ogura & Kondo 1970; Nield 1975).

2.3. *Perturbation analysis*

We consider perturbations around the base state:

$$\boldsymbol{u} = \boldsymbol{u}', \quad \boldsymbol{u}_G = \bar{w}_G \boldsymbol{e}_z + \boldsymbol{u}'_G, \quad \varepsilon_G = \bar{\varepsilon}_G + \varepsilon'_G, \tag{2.7a–c}$$

where perturbation components are indicated by primes. The velocity fields $\boldsymbol{u}'$ and $\boldsymbol{u}'_G$ are assumed 2-D: $\boldsymbol{u}' = u'\boldsymbol{e}_x + w'\boldsymbol{e}_z$, $\boldsymbol{u}'_G = u'_G\boldsymbol{e}_x + w'_G\boldsymbol{e}_z$. Substituting (2.7a–c) in (2.1) and (2.3), we have

$$\frac{\partial \varepsilon'_G}{\partial t} + \left(\bar{w}_G \frac{\partial}{\partial z} + \frac{d\bar{w}_G}{dz}\right)\varepsilon'_G + \bar{\varepsilon}_G \frac{\partial u'_G}{\partial x} + \left(\bar{\varepsilon}_G \frac{\partial}{\partial z} + \frac{d\bar{\varepsilon}_G}{dz}\right)w'_G + \boldsymbol{\nabla} \cdot (\varepsilon'_G \boldsymbol{u}'_G) = 0, \tag{2.8a}$$

$$\frac{\partial \boldsymbol{u}'_G}{\partial t} + \bar{w}_G \frac{\partial \boldsymbol{u}'_G}{\partial z} + \frac{d\bar{w}_G}{dz}w'_G \boldsymbol{e}_z + \boldsymbol{u}'_G \cdot \boldsymbol{\nabla}\boldsymbol{u}'_G$$
$$= 3\left(\frac{\partial \boldsymbol{u}'}{\partial t} + \boldsymbol{u}' \cdot \boldsymbol{\nabla}\boldsymbol{u}'\right) - \frac{18}{r_b^2}(\boldsymbol{u}'_G - \boldsymbol{u}') + (\bar{w}_G + w'_G - w')\zeta'\boldsymbol{e}_x - (u'_G - u')\zeta'\boldsymbol{e}_z, \tag{2.8b}$$

$$\boldsymbol{\nabla} \cdot \boldsymbol{u}' = \boldsymbol{0}, \tag{2.8c}$$

$$\frac{\partial \boldsymbol{u}'}{\partial t} + \boldsymbol{u}' \cdot \boldsymbol{\nabla}\boldsymbol{u}' = -\boldsymbol{\nabla}\pi' + \Delta\boldsymbol{u}' + \frac{Rar_b^2}{9Pr}(\bar{\varepsilon}_G + \varepsilon'_G)\left(\frac{\partial \boldsymbol{u}'}{\partial t} + \boldsymbol{u}' \cdot \boldsymbol{\nabla}\boldsymbol{u}'\right) + \varepsilon'_G \frac{Ra}{Pr^2}\boldsymbol{e}_z, \tag{2.8d}$$

$$\frac{\partial u'}{\partial z} + \frac{\partial w'}{\partial x} = w' = 0, \quad \text{at } z = 1, \tag{2.9a}$$

$$u' = w' = w'_G = \varepsilon'_G = 0, \quad \text{at } z = -1, \tag{2.9b}$$

where $\zeta' = \partial_z u' - \partial_x w'$ is the liquid vorticity perturbation and π' is the perturbation of a reduced pressure. To solve the set of (2.8) and (2.9), we assume travelling wave modes and

expand the perturbations $(\boldsymbol{u}'_G, \boldsymbol{u}', \varepsilon'_G)$ into the Fourier–Chebyshev series:

$$\left(\boldsymbol{u}'_G, \, \boldsymbol{u}', \, \varepsilon'_G\right) = \sum_{m=-\infty}^{\infty} \sum_{l=0}^{\infty} \left(\widehat{\boldsymbol{u}}_{G,m,l}, \, \widehat{\boldsymbol{u}}_{m,l}, \, \widehat{\varepsilon}_{G,m,l}\right) T_l(z) \exp(\mathrm{i}m\alpha(x - ct)), \quad (2.10)$$

where $T_l(z)$ is the Chebyshev polynomial of degree l, α is the wavenumber of fundamental mode and c is the phase velocity. The case of $c = 0$ corresponds to a steady convection. Substituting (2.10) for perturbation fields in (2.8a)–(2.9b) and truncating the series at $m = \pm M$ and $l = L$, we obtain a set of coupled nonlinear algebraic equations for $\widehat{\boldsymbol{u}}_{G,m,l} = (\hat{u}'_{G,m,l}, \hat{w}'_{G,m,l})$, $\widehat{\boldsymbol{u}}_{m,l} = (\hat{u}'_{m,l}, \hat{w}'_{m,l})$, and $\widehat{\varepsilon}_{G,m,l}$ ($m = 0, \pm 1, \pm 2, \ldots, \pm M$; $l = 0, 1, \ldots, L$):

$$F_i = L_{ij}X_j + N^{(2)}_{ijk}X_jX_k + N^{(3)}_{ijkl}X_jX_kX_l + \mathrm{i}\alpha c\, C_{ij}X_j = 0, \quad (2.11)$$

where $\{X_j\} = \{\hat{u}'_{G,m,l}, \hat{v}'_{G,m,l}, \hat{u}'_{m,l}, \hat{w}'_{m,l}, \widehat{\varepsilon}_{G,m,l} \,|\, m = -M, \ldots, M; l = 0, 1, \ldots, L\}$ and L_{ij}, $N^{(2)}_{ijk}$, $N^{(3)}_{ijkl}$, and C_{ij} are coefficients. We solve these equations by the numerical continuation with varying Ra from the critical value (Dijkstra *et al.* 2014). To determine the solution at a given Ra, the Newton–Raphson iterative scheme is invoked with a convergence criterion $\Delta = \max_j(\Delta_j) < 10^{-6}$, where Δ_j is the relative improvement to $(I - 1)$th estimate X_j^{I-1} to X_j by the Ith iteration (Deguchi & Nagata 2011). The improvement Δ_j is defined as $\Delta_j = |(X_j^I - X_j^{I-1})/X_j^{I-1}|$ when $|X_j^I|, |X_j^{I-1}| > 10^{-6}$; $\Delta_j = 0$ otherwise. For the solutions computed under this criterion, (2.11) are satisfied with a tolerance of $O(10^{-8})$. The truncation parameters are fixed at $M = 25$ and $L = 35$ for convergence.

3. Nonlinear properties of the flows

3.1. *Bifurcation diagram*

We compute the flows developing from critical modes with varying Ra for different values of Pr in the range $0.56 \le Pr/Pr^* \le 2.3$, which was considered in Nakamura *et al.* (2020) for the linear stability analysis. The obtained bifurcation diagrams for a case of $Pr < Pr^*$ and another case of $Pr > Pr^*$ are shown in figure 2, where the behaviour of the solution is monitored through the variation of $\max(u')$ as a function of the bifurcation parameter $\delta = (Ra - Ra_c)/Ra_c$. Determined flows are all stationary ($c = 0$). Flow fields at different points on the bifurcation curves are also shown. For the whole-layered mode ($Pr < Pr^*$), the convection develops through a subcritical bifurcation (figure 2a). The curve revolves once δ goes down to -0.3 and, then, δ starts increasing with $\max(u')$. For the multi-layered mode ($Pr > Pr^*$), in contrast, the flow grows through a supercritical bifurcation (figure 2b). A revolution occurs at approximately $\delta = 0.02$ and, then, $\max(u')$ continues to increase but with decreasing δ. In both cases, pairs of equally sized convection rolls develop at weak nonlinearity, i.e. at small $\max(u')$, as shown in figure 2(a1,b1,b2). Sharp ascending plumes are observed at large $\max(u')$, see figure 2(a2,a3,b3). These plumes are coincident with bubble-concentrated zones and delimited laterally by bubble-poor zones.

We have examined the effects of the drag force model on bifurcations by determining bifurcation diagrams with $C_D = 16/Re_b$ (Hadamard 1911; Rybczynski 1911) and $C_D = 24/Re_b$ (Stokes 1851). The former and latter models are valid in the low-Reynolds-number limit for bubbles in a pure liquid and for bubbles in a liquid contaminated by surfactants, respectively. In all cases, the bifurcations of whole- and multi-layered critical modes are found to be subcritical and supercritical, respectively.
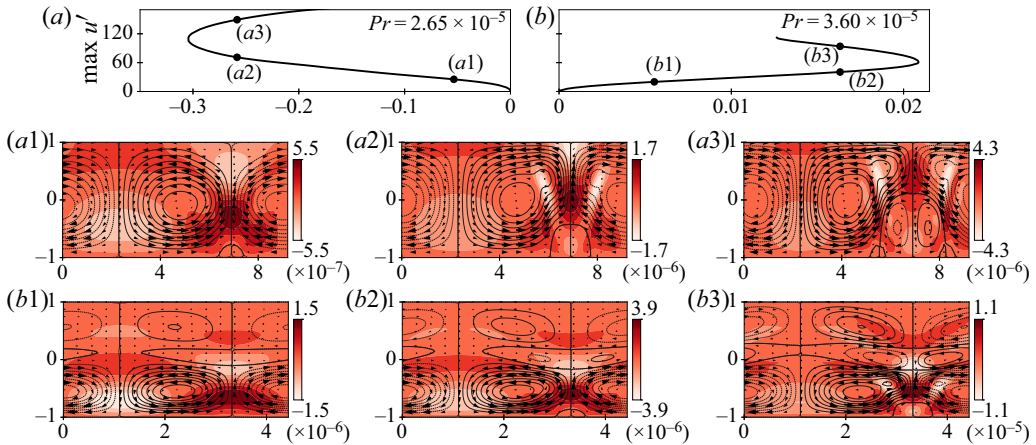
Figure 2. Bifurcation diagrams for (*a*) the whole-layered mode and (*b*) the multi-layered mode: (*a*1–*a*3; *b*1–*b*3) flow patterns at different points in the diagrams: the bifurcation parameter δ is defined by $\delta = (Ra - Ra_c)/Ra_c$ with $Ra_c = 337$ and 764 for (*a*) and (*b*), respectively. The ordinates max u' are the maximum horizontal velocity of the liquid phase. In panels (*a*1–*a*3) and (*b*1–*b*3), the liquid velocity fields $\boldsymbol{u}'$ are shown by arrows and streamlines. The gas volume fraction fields ε'_G are shown by colours.

3.2. *Energy budget*

Nakamura *et al.* (2020) showed essential differences between the instabilities of thermal and bubble-induced convections by an energy budget analysis. Both convections result from heterogeneous distribution of buoyancy sources, i.e. the temperature and the gas fraction in thermal and bubble-induced convections, respectively. However, the transport processes of these sources and resulting effects are distinct from each other. In thermal convection, the advection and diffusion of thermal energy bring about destabilising and stabilising effects, respectively. In bubble-induced convection, the lift and drag forces on bubbles tend to homogenise bubble distributions and, as a consequence, to stabilise the base state, while the inertial effect of liquid brings about destabilising effects.

We perform a similar energy budget analysis to consider the energy transfer from the base to perturbation flows and to reveal the driving mechanism of convective flows. Since (2.8*b*) and (2.8*c*) governing the liquid phase dynamics are analogous to the corresponding equations for thermal convection (Drazin & Reid 2010), the energy transfer to liquid perturbation flows is similar to that in the RB convection: the flows gain and lose energy due to buoyancy and viscous energy dissipation, respectively. The energy transfer to perturbation flows of the gas phase is more insightful. Taking the inner product of (2.8*b*) with $\boldsymbol{u}'_G$ and averaging the resulting equation over the whole fluid domain, we obtain the evolution equation of the kinetic energy of the gas phase:

$$\frac{\mathrm{d}K_G}{\mathrm{d}t} = W_I + W_D + W_L, \tag{3.1}$$

where the kinetic energy K_G and the powers of the inertia W_I, of the drag W_D and of the lift W_L are defined by

$$K_G = \left\langle \frac{u'^2_G + w'^2_G}{2} \right\rangle, \quad W_I = \langle w_I \rangle, \quad W_D = \langle w_D \rangle, \quad W_L = \langle w_L \rangle, \tag{3.2a}$$
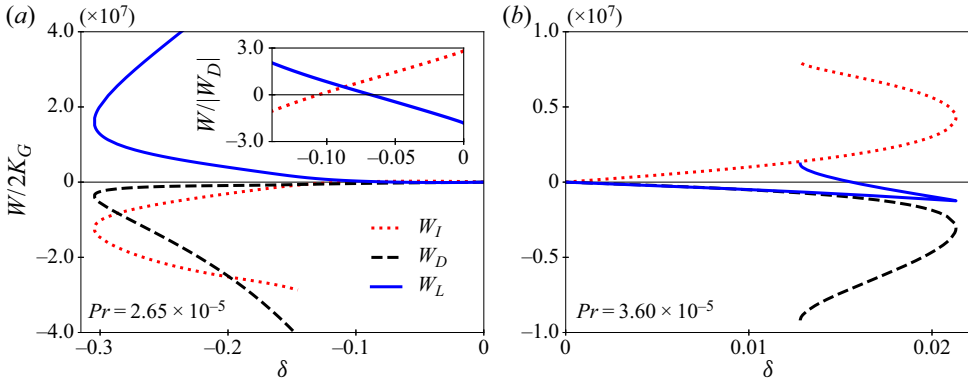
923 R4-7

Figure 3. Energy transfer from the base to perturbation flows of gas phase for (*a*) whole-layered modes and (*b*) multi-layered modes. The powers W_I, W_D and W_L of the inertia, drag and lift forces are shown in function of the bifurcation parameter δ. These powers are normalised by twice the kinetic energy K_G of gas perturbation flows. In panel (*a*), the powers W_I and W_L normalised by $|W_D|$ are also shown as inset for $\delta \in [-0.15, 0]$.

with

$$
w_I = -\left[\bar{w}_G \frac{\partial}{\partial z} \frac{\|\boldsymbol{u}'_G\|^2}{2} + \frac{d\bar{w}_G}{dz} w_G'^2 + (\boldsymbol{u}'_G \cdot \boldsymbol{\nabla} \boldsymbol{u}'_G) \cdot \boldsymbol{u}'_G \right]
$$
$$
+ 3\left[\frac{\partial \boldsymbol{u}'}{\partial t} \cdot \boldsymbol{u}'_G + (\boldsymbol{u}' \cdot \boldsymbol{\nabla} \boldsymbol{u}') \cdot \boldsymbol{u}'_G \right], \tag{3.2b}
$$

$$
w_D = -\frac{18}{r_b^2}(\boldsymbol{u}'_G - \boldsymbol{u}') \cdot \boldsymbol{u}'_G, \quad w_L = \bar{w}_G \zeta' u'_G + (u'w'_G - w'u'_G)\zeta'. \tag{3.2c}
$$

The angle brackets denote the following integral operation: $\langle \bullet \rangle = (\alpha/2\pi) \int_{-1}^{1} \int_0^{2\pi/\alpha} \bullet\, dx\, dz$. The integrands w_I, w_D and w_L are local densities of the inertia, drag and lift powers.

For both whole- and multi-layered convective flows, the drag is impeding ($W_D < 0$) convective flows (figure 3). The roles of the inertia and lift, however, depend on the mode type and can vary with the flow nonlinearity. In the case of the whole-layered flows (figure 3*a*), the inertia and lift forces are, respectively, driving ($W_I > 0$) and impeding ($W_L < 0$) convections close to the critical state as observed in the linear stability analysis (Nakamura *et al.* 2020). However, these effects relative to the drag force, i.e. the effects measured by $W_I/|W_D|$ and $W_L/|W_D|$, diminish and increase with the flow development, as shown in the inset of figure 3(*a*). This implies that the lift plays an important role to drive convection at *Ra* smaller than the critical value. In the case of the multi-layered modes, the powers of inertia and lift forces remain, respectively, positive and negative during the flow development along the bifurcation curve (figure 3*b*). Around the revolution of the curve, however, the effect of the lift relative to the drag decreases and switches finally to a driving one.

4. Discussion

The sensitivity of nonlinear development of convections to the constitutive law of fluid is reported in the literature for thermal convections under different conditions: Parmentier (1978), Solomatov (2012) and Curbelo & Mancho (2014) for Newtonian
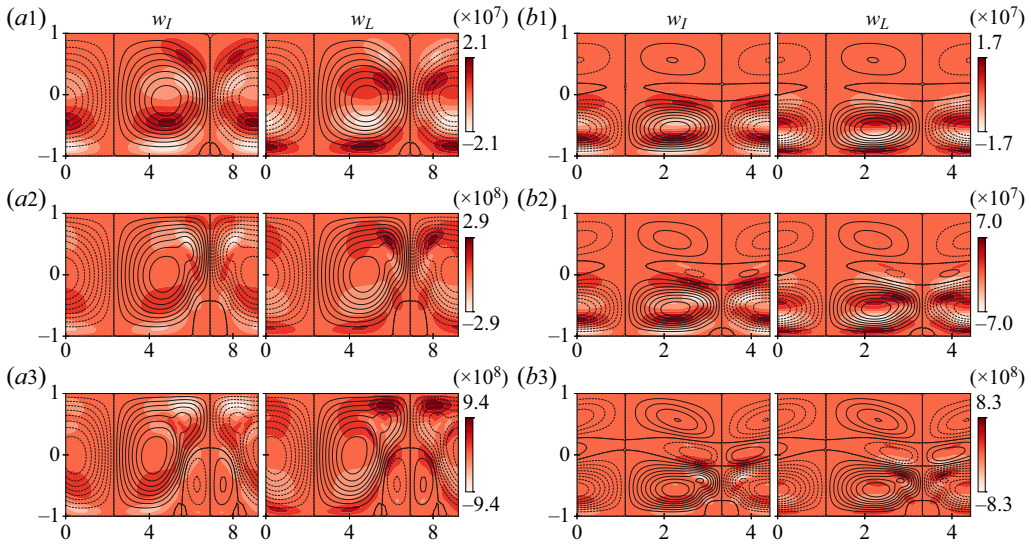
923 R4-8

Figure 4. Local power densities, w_I of the inertia and w_L of the lift, providing energy to perturbation gas flows in flows shown in figures 2(*a*1–*a*3) and 2(*b*1–*b*3).

fluids with a temperature-dependent viscosity; Albaalbaki & Khayat (2011), Benouared, Mamou & Messaoudene (2014) and Bouteraa *et al.* (2015) for non-Newtonian fluids with shear-thinning effects; and Kang *et al.* (2021) for suspensions with an effective viscosity modelled by Krieger's law. The results reported in § 3.1 (figure 2*a*,*b*) suggest that the bifurcation can also be altered by the law of transport of dispersed phase. As we have assumed dilute bubbly flows, the presence of bubbles has no rheological effect in contrast to the above-mentioned works on convections and affects the liquid dynamics only through the buoyancy force (2.1*d*). The essential difference of the considered system compared with thermal convections arises from the transport equation of bubbles (2.1*b*). The energy budget analysis in § 3.2 indicates a significant role of the lift force in sustaining convective flows. The power provided by the lift force behaves differently in different bifurcations (figure 3). The details of energy transfer process can be understood from the local distributions of different powers (figure 4). In the case of subcritical bifurcation, the complex coupling of the bubble transport law (2.1*d*) with developed convective flows intensifies the driving effect of the lift ($w_L > 0$) close to the free surface and weakens the impeding effect of the lift ($w_L < 0$) in the lower part of convection rolls (figure 4*a*). It results in the change of net effect of the lift force from impeding ($W_L < 0$) to driving ($W_L > 0$) convective flows. The distribution of the power of the inertia (w_I) is similar to w_L but with the opposite sign. In the case of supercritical bifurcation, the distribution of w_L behaves differently (figure 4*b*). Though the development of positive and negative zones of w_L in the first convection layer at the bottom is similar to the subcritical case, negative zones of w_L grow in the second convection layer (figure 4*b*). The total effect of the lift, thus, remains impeding even after the revolution of the bifurcation curve.

Dispersed phase can thus change the bifurcation through the variations of different forces in its transport law. Laminar-turbulent transition in multi-phase flows would be affected by this mechanism. In experiments on the transition in particle-laden pipe flows, the transition from the laminar flow was observed to be supercritical at large values of particle volume fraction ϕ in contrast to the subcritical bifurcation of the Newtonian

Hagen–Poiseuille flow (Hogendoorn & Poelma 2018; Agrawal, Choueiri & Hof 2019). To model this transition, a thorough consideration on particle transport might be required in addition to a rheological consideration.

In the present study, only 2-D flows are considered, assuming a fluid layer of infinite horizontal extent. The presence of lateral boundaries can develop three dimensional (3-D) flow structures even at the first bifurcation point as observed in thermal convection (Dijkstra *et al.* 2014). In bubbly flow systems, furthermore, the physics at bubble scales, such as the path instability and bubble–bubble interactions (Risso 2018), provides 3-D perturbations to flows and would induce transition to 3-D convections even in laterally non-confined systems. The bifurcation to 3-D flows is to be examined in a future work.

5. Conclusion

In the present paper, we have investigated the nonlinear development of bubble-induced convection from the critical states predicted in our previous work (Nakamura *et al.* 2020). Bifurcations determined for the whole- and multi-layered modes, which are critical for the bubble Prandtl number Pr smaller and larger than Pr^*, are subcritical and supercritical, respectively.

We have analysed the energy transfer from the base to perturbation flows of the gas phase. The analysis revealed that the bubble transports due to different forces play important roles in the nonlinear development of convection. In particular, the lift force changes its role from impeding to driving convective flows when the convection is intensified with decreasing control parameter. It is responsible for the observed subcritical behaviour of the convection. Local effects of different transport mechanisms showed that the variation in the role of the lift arises from the coupling of gas transport with nonlinear liquid flows.

The observed sensitivity of flow bifurcation to the transport of dispersed phase suggests that, in addition to the rheological effects, a thorough consideration on the transport would be required for modelling laminar-turbulent transitions in multi-phase flow systems.

Declaration of interests. The authors report no conflict of interest.

Author ORCIDs.
- Kotaro Nakamura https://orcid.org/0000-0002-9039-962X;
- Harunori N. Yoshikawa https://orcid.org/0000-0003-4472-4425;
- Yuji Tasaka https://orcid.org/0000-0002-8943-4803;
- Yuichi Murai https://orcid.org/0000-0002-6835-9277.

REFERENCES

AGRAWAL, N., CHOUEIRI, G.H. & HOF, B. 2019 Transition to turbulence in particle laden flows. *Phys. Rev. Lett.* **122** (11), 114502.

ALBAALBAKI, B. & KHAYAT, R.E. 2011 Pattern selection in the thermal convection of non-Newtonian fluids. *J. Fluid Mech.* **668**, 500–550.

BENOUARED, O., MAMOU, M. & MESSAOUDENE, N.A. 2014 Numerical nonlinear analysis of subcritical Rayleigh–Bénard convection in a horizontal confined enclosure filled with non-Newtonian fluids. *Phys. Fluids* **26**, 073101.

BOUTERAA, M., NOUAR, C., PLAUT, E., METIVIER, C. & KLACK, A. 2015 Weakly nonlinear analysis of Rayleigh–Bénard convection in shear-thinning fluids: nature of the bifurcation and pattern selection. *J. Fluid Mech.* **767**, 696–734.

CLIFT, R., GRACE, J.R. & WEBER, M.E. 2005 *Bubbles, Drops, and Particles*. Courier Corporation.

CLIMENT, E. & MAGNAUDET, J. 1999 Large-scale simulations of bubble-induced convection in a liquid layer. *Phys. Rev. Lett.* **82** (24), 4827.

CURBELO, J. & MANCHO, A.M. 2014 Spectral numerical schemes for time-dependent convection with viscosity dependent on temperature. *Commun. Nonlinear Sci. Numer. Simul.* **19**, 538–553.

DEGUCHI, K. & NAGATA, M. 2011 Bifurcations and instabilities in sliding Couette flow. *J. Fluid Mech.* **678**, 156–178.

DIJKSTRA, H., *et al.* 2014 Numerical bifurcation methods and their application to fluid dynamics: analysis beyond simulation. *Commun. Comput. Phys.* **15** (1), 1–45.

DRAZIN, P.G. & REID, W.H. 2010 *Hydrodynamic Stability*. Cambridge University Press.

DRUZHININ, O.A. & ELGHOBASHI, S. 1998 Direct numerical simulation of bubble-laden turbulent flows using the two fluid formulation. *Phys. Fluids* **10** (3), 685–697.

HADAMARD, J. 1911 Mouvement permanent lent d'une sphere liquid et visqueuse dans un liquide visqueux. *C. R. Acad. Sci.* **152**, 1735–1738.

HOGENDOORN, W. & POELMA, C. 2018 Particle-laden pipe flows at high volume fractions show transition without puffs. *Phys. Rev. Lett.* **121** (19), 194501.

IGA, K. & KIMURA, R. 2007 Convection driven by collective buoyancy of microbubbles. *Fluid Dyn. Res.* **39** (1–3), 68–97.

KANG, C., YOSHIKAWA, H.N. & MIRBOD, P. 2021 Onset of thermal convection in non-colloidal suspensions. *J. Fluid Mech.* **915**, A128.

LEVICH, V.G. 1962 *Physicochemical Hydrodynamics*. Prentice-Hall.

LOHSE, D. 2018 Bubble puzzles: from fundamentals to applications. *Phys. Rev. Fluids* **3** (11), 110504.

MAGNAUDET, J. & EAMES, I. 2000 The motion of high-Reynolds-number bubbles in inhomogeneous flows. *Annu. Rev. Fluid Mech.* **32** (1), 659–708.

MUDDE, R.F. 2005 Gravity-driven bubbly flows. *Annu. Rev. Fluid Mech.* **37**, 393–423.

NAKAMURA, K., YOSHIKAWA, H.N., TASAKA, Y. & MURAI, Y. 2020 Linear stability analysis of bubble-induced convection in a horizontal liquid layer. *Phys. Rev.* E **102**, 053102.

NIELD, D.A. 1975 The onset of transient convective instability. *J. Fluid Mech.* **71** (3), 441–454.

OGURA, Y. & KONDO, H. 1970 A linear stability of convective motion in a thermally unstable layer below a stable region. *J. Met. Soc. Japan* **48** (3), 204–216.

PARMENTIER, E.M. 1978 A study of thermal convection in non-Newtonian fluids. *J. Fluid Mech.* **84** (1), 1–11.

RISSO, F. 2018 Agitation, mixing, and transfers induced by bubbles. *Annu. Rev. Fluid Mech.* **50**, 25–48.

RUZICKA, M.C. 2013 On stability of a bubble column. *Chem. Engng Res. Des.* **91** (2), 191–203.

RUZICKA, M.C. & THOMAS, N.H. 2003 Buoyancy-driven instability of bubbly layers: analogy with thermal convection. *Intl J. Multiphase Flow* **29** (2), 249–270.

RYBCZYNSKI, W. 1911 Uber die fortschreitende Bewegung einer flussigen Kugel in einem zahen Medium. *Bull. Acad. Sci.* **1**, 40–46.

SOLOMATOV, V.S. 2012 Localized subcritical convective cells in temperature-dependent viscosity fluids. *Phys. Earth Planet. Inter.* **200–201**, 63–71.

SOMMERFELD, M. 2004 *Bubbly Flows: Analysis, Modelling and Calculation*. Springer.

STOKES, G.G. 1851 On the effect of the internal friction of fluids on the motion of pendulums. *Trans. Camb. Phil. Soc.* **IX**, 8.